SLS-TME-TA-2008-0311
15th July 2008

Halo background in SLS-FEMTO

Andreas Streun

Paul Scherrer Institut, CH-5232 Villigen PSI, Switzerland

A proposed upgrade of the laser slicing repetition frequency to increase the flux for FEMTO also increases the background noise of the experiment, because the laser repetition time is much shorter than the radiation damping time, leading to a formation of an equilibrium beam halo. An analytical estimate of the noise to signal ratio as a function of laser repetition rate is derived and compared to an alternative estimate.

Halo background in SLS-FEMTO

Introduction

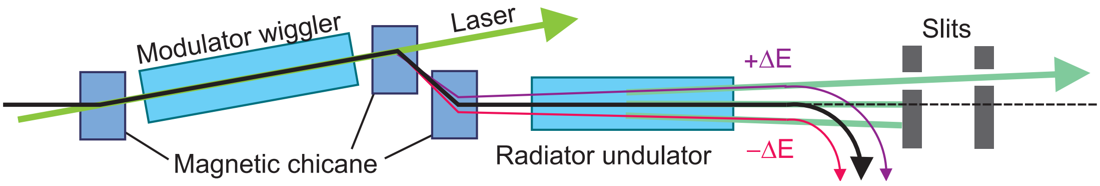

Figure 1: Schematic layout of the FEMTO beamline.

Laser beam interaction in the modulator wiggler introduces an energy modulation in a thin slice of the bunch. The dispersion of the magnetic chicane transfers the energy modulation to a horizontal amplitude in order to separate the short satellite bunches laterally from the core beam. The radiation from one of the satellites is then extracted by a system of apertures (slits) whereas the radiation from the core beam and from the chicane magnets and ring dipoles is blocked.

Since the laser repetition time is shorter than the horizontal radiation damping time, the satellite does merge back into the core beam before the next laser beam interaction. But due to the dependancy of the betatron tune on energy and amplitude it filaments and forms a beam halo. Some amount of the halo radiation will be transmitted by the apertures of the beamline and provide an unwanted background signal. Depending on the laser repetition time, the halo is composed from the relics from a number of previous laser beam interactions. The total halo radiation accepted by the beamline determines the noise-to-signal (N/S) ratio of the experiment.

An upgrade of laser repetition rate from the present 2 kHz to 10 kHz is planned to increase the flux for FEMTO. Before purchasing a new laser, the N/S as a function of laser repetition rate has to be calculated.

An early study [7] using a rather crude model of constant energy offset of the satellite particles already revealed the processes of halo formation and decay. A recent analysis [4] using a more detailed Gaussian distribution model came to conclusions which agree with this study, which uses an alternative linear distribution model.

Beamline acceptance

Several slits filter the photons in order to extract the radiation of one of the satellites and suppress static background from the core beam, chicane magnets etc. and dynamic background from the beam halo. Fig. 2 shows a backtransformation of the slits to the midpoint of the radiator undulator, given by

$$\begin{pmatrix} x \\ x' \end{pmatrix}_{L,H} = \begin{pmatrix} 1 & -L \\ 0 & 1 \end{pmatrix} \cdot \begin{pmatrix} s_{L,H} \\ \lambda \end{pmatrix} \qquad \lambda \in \boldsymbol{R}, \tag{1}$$

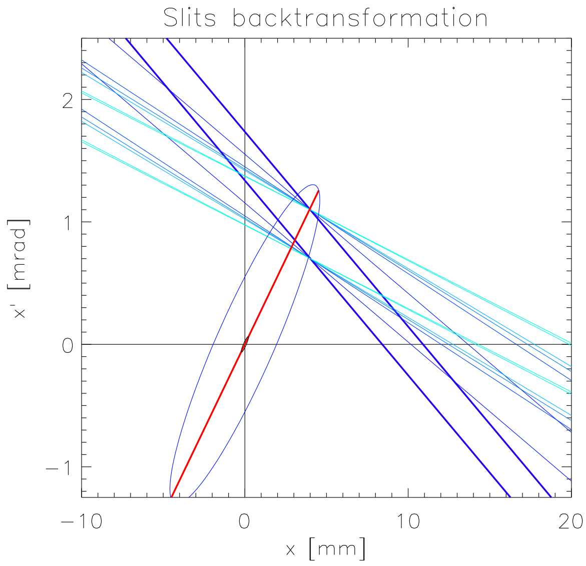

Figure 2: Acceptance definition by aperture slits
Backtransformation of the aperture slits to the radiator centre. The red bar shows the initial beam distribution, the large ellipse confines the beam halo. The small black ellipse at the origin corresponds to the 1σ equilibrium beam emittance.

where L ist the distance of the slit from the radiator center, and s_L, s_H are the horizontal positions of the inner and outer blades, defining lowest and highest accepted energy. Also shown in fig. 2 is the transformation of the laser induced energy modulation to the radiator centre (red line), where it has translated to horizontal offset and angle due to dispersion. Neglecting the beam emittance contributions is well justified when comparing the dispersion's contribution to the equilibrium beam size. This makes the modulated beam distribution essentially 1-dimensional, because x and x' are determined by dispersion and thus correlated. It is given by eq.(3) in [8]:

$$\begin{pmatrix} x \\ x' \end{pmatrix} = \sqrt{\mathcal{H}}\delta \cdot \begin{pmatrix} \sqrt{\beta_u} & 0 \\ -\alpha/\sqrt{\beta} & 1/\sqrt{\beta} \end{pmatrix} \cdot \begin{pmatrix} \cos(\Psi - \Phi) \\ \sin(\Psi - \Phi) \end{pmatrix}, \tag{2}$$

with the dispersion's emittance at wiggler exit given by

$$\text{with } \mathcal{H} = \gamma_w \eta_w^2 + 2\alpha_w \eta_w \eta_w' + \beta_w \eta_w'^2 \tag{3}$$

and $\delta = \Delta E/E$ the relative energy modulation, reaching up to a maximum value δ_o given by the energy of the laser pulse. α, β, γ are the Twiss parameters and η, η' the dispersion and its derivative. Index w refers to the wiggler exit, no index refers to the radiator undulator midpoint. Φ is the betatron phase advance from wiggler to undulator and Ψ is the initial betatron phase of the satellite given by [8]

$$\Psi = \arctan\left(\frac{\alpha_w \eta_w + \beta_w \eta_w'}{\eta_w}\right) - \pi. \tag{4}$$

In the turns following the laser shot, the beam will rotate in phase space following the contour of the large ellipse shown in fig. 2. Due to filamentation it will cover the ellipse area, i.e. form a beam halo relatively fast, within less than 100 turns, i.e. before the next laser shot: 10 kHz laser repetition rate correspond to a shot every 104 turns. Due to radiation damping the ellipse will shrink relatively slow: horizontal damping time in SLS is $\tau_x = 8$ ms corresponding to 80 laser shots at 10 kHz repetition rate. All ellipse area inside the acceptance parallogram will contribute to the background noise. As it can be seen in fig. 2 it is mainly the first slit (shown as a pair of thick lines), that determines the acceptance, so in order to simplify further considerations, we use only this one slit.

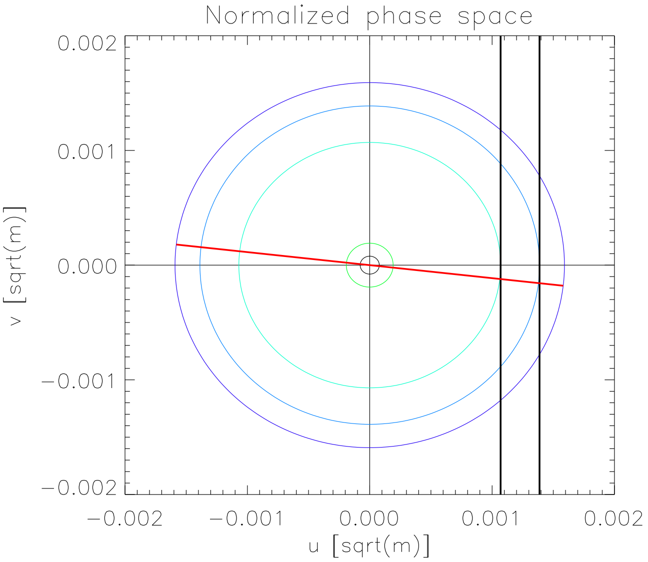

Figure 3: Halo acceptance in normalized phase space

The situation from fig. 2 in normalized phase space, where the beam ellipse appears as a circle and the dominant slit as a corridor parallel to one of the axis. The small black circle in the centre corresponds to the 1σ beam emittance, the medium circles to the amplitudes $a_{L,H}$ defining the acceptance range.

We perform a transformation to a coordinate system (u, v) where a) the beam ellipse becomes a circle (normalized phase space coordinates) and b) where the slit extends in v-direction. This requires an additional rotation by an angle ξ given by

$$\tan\xi = \frac{L}{\beta - \alpha L}, \tag{5}$$

and we arrive at the situation shown in fig. 3. The transformation is described by

$$\begin{pmatrix} u \\ v \end{pmatrix} = \begin{pmatrix} \cos\xi & \sin\xi \\ -\sin\xi & \cos\xi \end{pmatrix} \cdot \begin{pmatrix} 1/\sqrt{\beta} & 0 \\ \alpha/\sqrt{\beta} & \sqrt{\beta} \end{pmatrix} \cdot \begin{pmatrix} x \\ x' \end{pmatrix} \tag{6}$$

The radius of a circle is given by the betatron amplitude of a particle, propagating on this circle at an angle of $2\pi/Q$ per turn, where Q is the machine tune. The amplitude is determined by the energy modulation and positive by definition:

$$a = \sqrt{\mathcal{H}_w \delta^2} > 0 \tag{7}$$

The beam ellipse of amplitude a_o has been transformed into the largest circle in fig. 3. Inserting eq.1 into eq.6 gives the the blade location in the new system:

$$u_{L,H} = \frac{s_{L,H}}{\sqrt{\beta_s}} \quad \text{with} \quad \beta_s = \sqrt{\beta - 2\alpha L + \gamma L^2} \tag{8}$$

the betafunction of the photon beam at the slit location. The amplitudes a accepted by the slit are then given by

$$a_L < a < a_H \quad \text{with} \quad a_{L,H} = u_{L,H}$$

Inserting the initial coordinates from eq.2 in eq.6 results in

$$\begin{pmatrix} u \\ v \end{pmatrix} = a \cdot \begin{pmatrix} \cos\mu \\ \sin\mu \end{pmatrix} \qquad \text{with} \quad \mu = \Psi - \Phi - \xi \tag{9}$$

Optimum signal acceptance requires $\mu = 0$ or $\mu = \pi$ as obvious from fig. 3. The particle distribution of the fully developed halo will be will be purely radial and isotropic in polar angle.

Initial transverse distribution

The energy distribution of the satellite beam after laser interaction as shown in fig. 4 in the region of the accepting slit may be well approximated by a linear function (normalized to unity):

$$\frac{dN}{d\delta} = \frac{1}{\delta_o}\left(1 - \frac{|\delta|}{\delta_o}\right), \qquad |\delta| \leq \delta_o \tag{10}$$

We are not interested in the core region, since this will always be blocked. According to eq.7 the distribution in amplitudes is identical to the energy distribution, except the factor 2, because $a > 0$ by definition:

$$\frac{dN}{da} = \frac{2}{a_o}\left(1 - \frac{a}{a_o}\right). \tag{11}$$

We have to integrate over this distribution as it projects onto the slit interval as obvious from fig. 3 in order to obtain the desired signal immediately after interaction. But, other than later for the halo, only the amplitudes corresponding to $\delta > 0$ are accepted now, which requires to take only $1/2$ of the integral over the amplitudes from eq.11:

$$N_o = \frac{1}{2}\int_{a_L/\cos\mu}^{a_H/\cos\mu} \frac{dN}{da}\, da = \frac{1}{a_o}\left(\frac{a_H - a_L}{\cos\mu} - \frac{a_H^2 - a_L^2}{2a_o\cos^2\mu}\right) \tag{12}$$

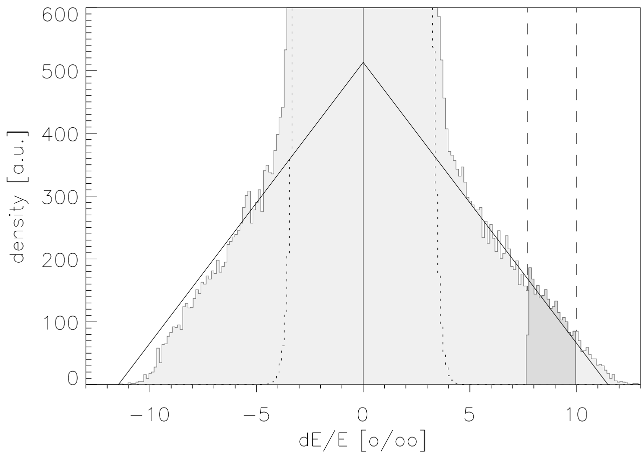

Figure 4: Particle distribution as a function of energy.
The core beam distribution alone (before laser modulation) is shown as dotted line. A slit in the beam line defines an interval of electron energy (dashed lines) from which the emitted photons are accepted. The distribution is well approximated by a linear function (triangle). The histogram is based on simulation data [1] for 3 mJ laser energy.

with μ from eq.9. In later turns we get filamentation. This does not change the radial distribution (as long as we do not yet consider radiation damping) but smears it out over the complete polar angle. The radial integral over the beam distribution thus has to be weighted with the angle cut out by the slit for some radius a: From fig. 3 this angle for the inner/outer blade of the slit is given by

$$\phi_{L,H} = 2 \arccos\left(\frac{a_{L,H}}{a}\right) \tag{13}$$

Introducing the function

$$\begin{aligned} F(x,y) &= \frac{2}{y}\int_x^y \arccos\left(\frac{x}{u}\right)\cdot\left(1-\frac{u}{y}\right)\,du \\ &= \arccos z + z\left(\sqrt{1-z^2} - 2\ln\left(\frac{1+\sqrt{1-z^2}}{z}\right)\right), \qquad z := \frac{x}{y}, \end{aligned} \tag{14}$$

the accepted part of the halo can be written as

$$N = \frac{1}{\pi}\cdot\begin{cases} F(a_L,a_o) - F(a_H,a_0) & \text{if} \quad a_o > a_H \\ F(a_L,a_o) & \text{if} \quad a_L < a_o < a_H \\ 0 & \text{if} \quad a_L > a_o \end{cases} \tag{15}$$

Due to radiation damping the halo shrinks, i.e. $a_o = a_o(t)$ and finally approaches the equilibrium beam parameters of the core beam. As long as $a_o >> \sqrt{\epsilon}$ the linear distribution will be maintained, because the dynamics far above equilibrium is governed by pure classical damping with damping time τ. Since we are not interested in the core region, because $a_L >> \sqrt{\epsilon}$, we approximate the final Gaussian by a linear distribution of equal standard deviation which is given by

$$\sigma_a := a_o(t \to \infty) = \sqrt{6\epsilon} \tag{16}$$

and shown in fig. 3 as a small green circle. We measure time by number of shots n of the laser with repetition time T and write for the time dependancy of the halo amplitude:

$$a_n := a_o(t) = (a_{oo} - \sigma_a)e^{-nT/\tau} + \sigma_a \qquad (\ a_{oo} := a_o(0)\ ) \tag{17}$$

This defines two laser shot numbers n_H, n_L indicating the shots where the halo is not covered anymore by the outer blade, and where it is hidden completely by the inner blade:

$$n_{L,H} = \left[\frac{\tau}{T} \ln\left(\frac{a_{oo} - \sigma_a}{a_{L,H} - \sigma_a}\right)\right] \tag{18}$$

The total halo background thus is given by

$$N_{\text{halo}} = \frac{1}{\pi}\left(\sum_{n=1}^{n_L} F(a_L, a_n) - \sum_{n=n_H+1}^{n_L} F(a_H, a_n)\right) \tag{19}$$

Finally, the noise to signal ratio is given by normalizing to eq.12:

$$\text{N/S} = \frac{N_{\text{halo}}}{N_o} \tag{20}$$

Results

Based on simulations [1], the maximum energy modulation for the linear approximation was calculated:

Laser pulse energy	2	3	4	mJ
δ_o for eq.10	0.98	1.15	1.29	%

Using these data the halo decay curve as shown in fig.5 was established: it shows the single turn halo intensities $N(a_o(t))$ from eqs.15,17 normalized to the signal intensity N_o from eq.12. The N/S ratio as function of laser repetition rate is obtained from eq.20 and shown in table 1 for different laser energies:

Here, 2 mJ is an optimum case because $a_o \approx a_H$ gives best signal acceptance.(But this would be adjusted for other laser energies by moving the slits correspondingly.) Also shown in table 1 are the results from ref.[4] using a Gaussian approximation for the halo distribution.

However, the absolute N/S values are not too meaningful, because in reality, many parameters are optimized empirically to reduce N/S, which are not included in the

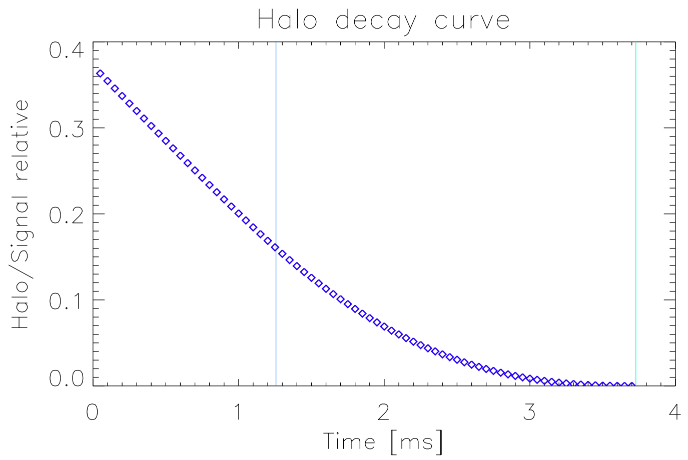

Figure 5: Halo decay curve

Accepted halo intensity normalized to the signal as a function of time. Due to radiation damping, the halo shrinks. The blue line marks the point where its outer region is not covered anymore by the outer blade, the green line, where it hidden completely by the inner blade. The diamonds correspond to the laser shots for 20 kHz repetition rate.

Table 1: Noise to signal ratio vs. laser repetition rate for different laser pulse energies

Laser repetition rate [kHz]		0.1	1	2	5	10	20	ratio 10/2
N/S from eq.20	2 mJ	0	0.10	0.34	1.09	2.36	4.90	7.0
	3 mJ	0	0.28	0.72	2.06	4.31	8.80	6.0
	4 mJ	0	0.52	1.23	3.39	7.00	14.2	5.7
N/S from ref.[4]	analytic			1.26		7.05	14.3	5.6
(2 mJ)	simulation			1.15		6.94		6.0

model. Presently the measured N/S amounts to only approx. 7% at a laser repetition rate of 2 kHz [2].

More important is the predicted increase of N/S for the proposed laser upgrade from 2 to 10 kHz repetition rate, shown in the last column of the table. Here we have general agreement predicting sixfold noise.

N/S as a function of laser repetition rate is shown in fig. 6 for 3 mJ laser energy. The linear dependancy is no surprise, because for relatively high laser repetition rate and large numbers of shots contributing to the halo, the halo decay curve from fig. 5 is just sampled more and more densely. The negative offset to the curve is due to zero halo intensity for very low repetition rate, where the halo disappears behind the inner blade due to damping before the next shot.

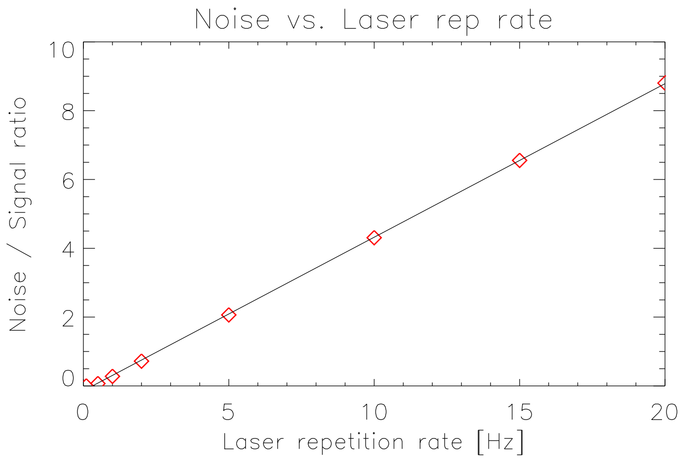

Figure 6: Noise to signal ratio vs. laser repetition rate
Data for 3 mJ laser pulse energy.

Alternative filling patterns

If the N/S ratio is too high, there is still the possibility to have several bunches in the ring and to slice them alternatingely. This would reduce N/S by the number of bunches. The gating of the detectors is sufficiently fast (≈ 20 ns). However, due to beam loading effects, mainly in the 3rd harmonic cavity, the filling pattern introduces an energy chirp, which is welcome basically, because it provides the Landau damping of coupled bunch instabilities, but it also leads to a temporal deviation of bunch centres of about $0.4 \ldots 0.7$ ps/bucket (depending on cavity tuning) at 400 mA. In order to have a constant repetition time T when alternating between several bunches (instead of a $T_1, T_2 \ldots$ series, which would be difficult to handle), the filling pattern needs a periodicity equal to the number of bunches to be sliced.

SLS has 480 buckets and is usually operated with a train of 390 bunches filled to about 1 mA plus a single bunch of triple current 30 ns in front of the train. The remaining gap (150 ns) is used for ion clearing. A feedback procedure based on individual bunches current measurements controls the filling pattern [3]. The system was recently upgraded to allow up to 5 mA (planned: up to 8 mA) single bunch current, and the feedback algorithm was improved. A quadruple-periodic filling pattern with 4 bunches of each about 4 mA for slicing and 4 trains of 75 bunches each as shown in fig. 7 was tested successfully in 400 mA top-up operation.

Conclusion

Increasing the laser repetion rate from 2 kHz to 10 kHz will increase the halo background six times, i.e. from the present $\approx 7\%$ to $\approx 40\%$. Alternating slicing of several bunches will be possible and reduce the background by the number of bunches.

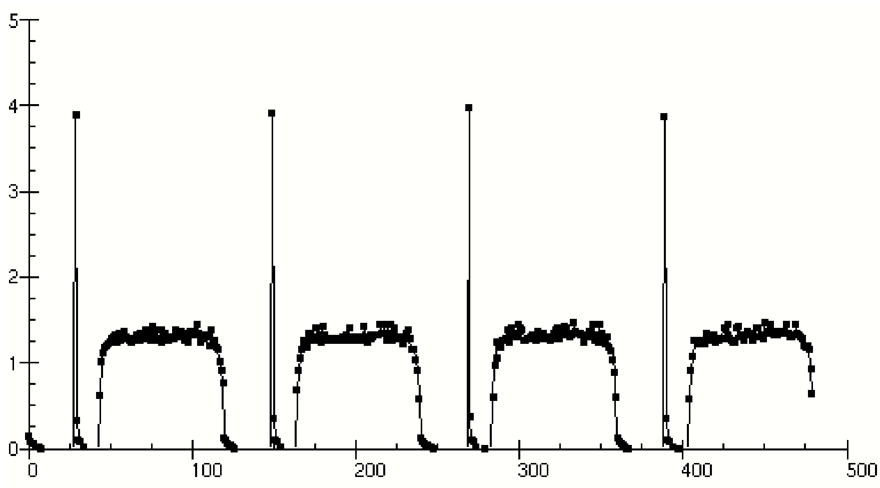

Figure 7: Filling pattern with 4 FEMTO bunches [5]

References

[1] P. Beaud, priv. comm.

[2] G. Ingold, priv. comm.

[3] B. Kalantari et al., "Bunch pattern control in top up mode at the SLS", Proc. EPAC 2004, p.2885.

[4] D. Kalantaryan et al., "The acceptance and photon beam formation in SLS FEMTO", Proc. EPAC 2008, Genova.

[5] SLS machine shift protocol from June 11, 2008.

[6] A.Streun et al., "Sub picosecond X-ray source FEMTO at SLS", Proc. EPAC 2006, Edinburgh, p.3427.

[7] A. Streun, "SLS-FEMTO: beam halo formation and maximum repetition rate for laser slicing",Internal Report SLS-TME-TA-2003-0222.

[8] A. Streun, "SLS-FEMTO: Chicane Layout, peformance and side-effects", Internal Report SLS-TME-TA-2003-0223.